2007

A Novel Setup For High-pressure Raman Spectroscopy Under A Microscope

Thomas Andrew Oakeson
University of Central Florida

A NOVEL SETUP FOR HIGH-PRESSURE RAMAN SPECTROSCOPY UNDER A MICROSCOPE

by

THOMAS ANDREW OAKESON
B.S. Brigham Young University, 2004

A thesis submitted in partial fulfillment of the requirements
for the degree of Master of Science
in the Department of Physics
in the College of Sciences
at the University of Central Florida
Orlando, Florida

Spring Term
2007

ABSTRACT

Functional properties of biological molecules and cells are affected by environmental parameters such as temperature and pressure. While Raman spectroscopy provides an intrinsic probe of molecular structural changes, the incorporation of a microscope enables studies of minuscule amounts of biological compounds with spatial resolution on a micron scale. We have developed a novel setup which combines a Raman microscope and a high pressure cell. A micro-capillary made out of fused silica simultaneously serves as the supporting body and the optical window of the pressure cell. The cell has been tested over the pressure range from 0.1 to 4 kbar. Raman spectra of less than 100 nanoliter amount of amino acid and protein solutions have been measured in the micro-capillary high pressure cell. It is also demonstrated that the setup is well suited for spectrally resolved fluorescence measurements at variable pressure.

ACKNOWLEDGMENTS

I would like to acknowledge and give my great appreciation for the help of my thesis advisor, Dr. Alfons Schulte, whose mentoring throughout my graduate schooling has been exceptional. I would like to give sincere thanks to Sang Hoon Park for the excellent, friendly, and reliable assistance that he has given me. I would like to thank the members of my thesis committee, Dr. Eduardo Mucciolo and Dr. Lee Chow, for both of whom having contributed to the positive graduate school experience that I've had. And a dear thank you to my family, whose support has been a tremendous blessing to me. Support of the Micro-Raman facility from NSF grant ECS-0123 484 is appreciated.

TABLE OF CONTENTS

LIST OF FIGURES

CHAPTER ONE: INTRODUCTION

Introducing high pressure to Raman Spectroscopy provides new opportunities of scientific research that are not available under other means. A high pressure environment (pressure used as a variable) allows experiments which give unique information about the microscopic properties of the materials that are studied. In particular, pressure can deactivate enzymes and kill bacteria.[1] Some sea creatures can function from sea level to extreme depth. Sharks, for example, encounter pressure from 0.1 MPa to 100 MPa. In order to understand these biological phenomena on a molecular level, the effects of pressure on isolated proteins must be understood. Investigations of the effects of pressure on proteins are a growing area of bio-physical research. It has been shown [2] that proteins undergo a pressure induced denaturation differently from that observed at high temperatures or in the presence of certain chemicals.

In the Biosciences, this high pressure environment holds a significant promise for study because pressure is an ideal parameter for reversible changes in biosystems, because "intermolecular non-covalent interactions dominate and determine their structure, dynamics and function." [3] Pressure changes, unlike temperature changes, are, in most cases, fully reversible. Indeed one of the most exciting aspects of high pressure studies is in the study of protein folding, unfolding and misfolding. Compression may play a role in the regulation of cell growth.[4] While the use of pressure to explore, at the molecular level, the dynamics and kinetics of transformations of materials, it is also being used to modify and improve qualities applicable to food processing. A new experimental method that we have been engaged in could well be a very

strong addition to the contributions that high-pressure studies in Bioscience are making. A detailed and full description of this method will be given in Chapter 3, but first a brief summary of our novel approach will follow here and conclude Chapter 1.

To be able to achieve the desired results in high pressure studies, a high pressure environment is required in the region of 2kbar to 8kbar. This obviously presents many difficulties due to the nature of pressures that high as well as the durability of pressure cells to withstand the pressure. But one simple and effective way to achieve this is with the use of silica (silicon dioxide) capillaries, which are similar to fiber optic tubing. Fig. [1] shows a cross-section of a capillary, also referred to as a "micro-capillary" due to its micron-scale dimensions. The cylindrical geometry of the capillary distributes stress evenly and thus has excellent pressure stability. The method of using capillaries as pressure cells was first accomplished by a group from the University of Illinois' Laboratory for Fluorescence Dynamics in 2002, using fluorescence correlation spectroscopy (FCS) as a probe.[3] This was motivated by the fact that "single molecule work requires microscope objectives with large numerical apertures, which have working distances of *less than one millimeter*." [3]

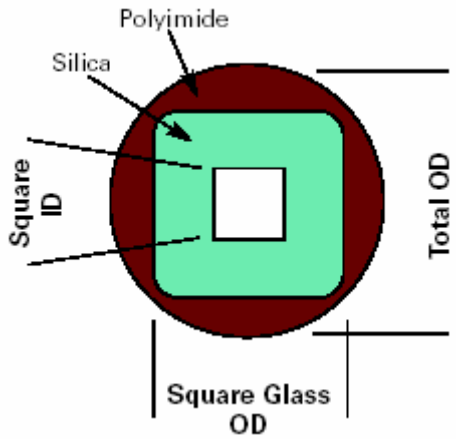

Figure 1: Cross section of micro-capillary (ID ≈ 50μm, OD ≈ 350μm)

A novel application using these micro-capillaries as high pressure cells for Raman spectroscopy under a microscope is developed in this thesis. Our objective is to go from an integral to a spectral probe and to develop a micro-capillary technique for high pressure applications of Raman Spectroscopy. A cell for micro-Raman Spectroscopy was constructed from scratch and the first measurements were conducted. This thesis is organized as follows: Chapter two will detail the theoretical aspects involved in our research to provide the scientific background encompassing our studies; chapter three will describe our high pressure Raman system in detail; and chapter four will present the data and results that we have collected from our high pressure Raman studies of biomolecules.

CHAPTER TWO: BACKGROUND ON EXPERIMENTAL TECHNIQUES

In chapter two I will discuss some of the basic theoretical aspects and the science involved in our study. It is appropriate to first provide some background on the thermodynamic effects on biomolecules, since, ultimately, the purpose of our research is to apply the very powerful, and yet remarkably simple, device for the study of biomolecules and protein dynamics. I will also be discussing the Raman effect and Raman Spectroscopy, to provide information on the important physical mechanisms involved, and the data-collecting instrument that is an integral part of our research method. Lastly, I will review some of the current experimental approaches to high-pressure studies which have led to our project.

2.1 Pressure Effects on Biomolecules

The study of the effects of pressure on biomolecules reveals a great deal about the dynamics and reactions of proteins. Since protein molecules can fluctuate among many different configurations, they possess many different conformational substates, which perform similar functions, but at different rates. The effect of pressure on protein molecules affects the functional properties of the individual substates, and hence large changes can occur in the dynamic properties of a protein ensemble. Pressure experiments on proteins have indicated a strong influence of conformational substates on protein reactions. As a thermodynamic variable, pressure is as important as temperature in the study of proteins. Pressure affects proteins in the following ways; it can act on a protein in a given substate, and it can shift the distribution of

substates, influencing protein structure, dynamics, and function, which are the conformational effects. Pressure changes protein structure and protein reaction rates.[5] Experiments that examine proteins while suddenly changing the pressure, known as "pressure jump experiments", reveal a number of relaxation processes of the proteins. [5] It has been shown that proteins undergo a pressure induced denaturation; they are affected in ways similar to those observed at high temperatures or in the presence of certain chemicals. The effects of pressure can also shift spectral lines.[6]

An understanding of the effects of pressure on proteins is most easily gained by considering a model for the simplest system resembling the mechanism of a protein. This protein would have two states, A and B, and two conformational substates, 0 and 1. Fig. [2] shows two cross sections through a highly simplified energy surface of a protein: at a constant conformational coordinate the protein possesses the two states A and B; and at a constant reaction coordinate the protein possesses two conformations, 0 and 1. In each of the two substates 0 and 1, the protein can make the transition B→A.

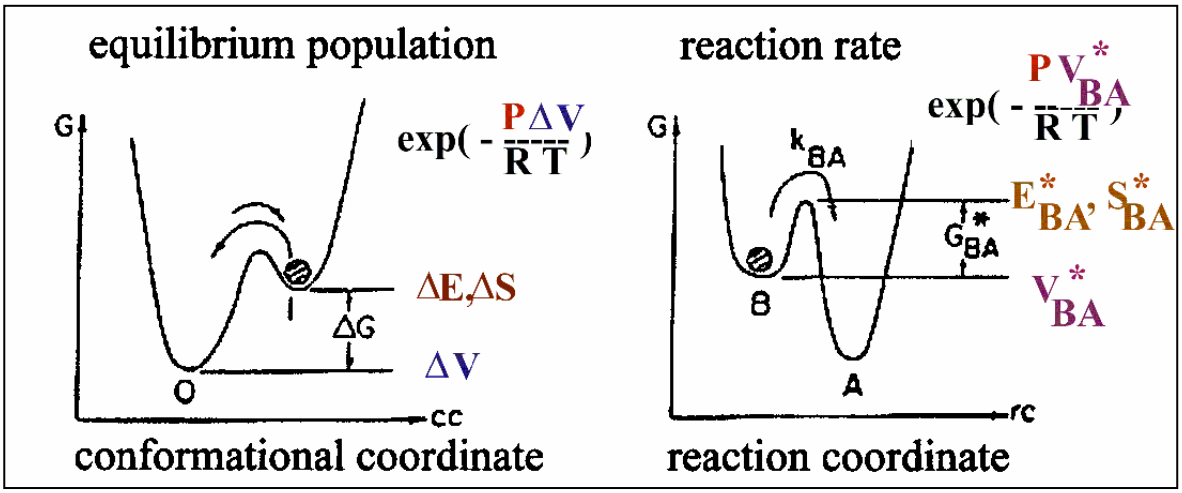

Figure 2: Schematic cross-sections through the free energy surface of a protein; panel (a) along a conformational coordinate, panel (b) along a reaction coordinate

Panel (a) of Fig. [2] shows the cross section through the energy surface at a constant reaction coordinate (rc=A). Panel (b) shows the cross section at constant conformational coordinate (cc=0). Pressure affects protein represented in Fig. [2] in two ways. In equilibrium, the ratio A_0/A_1 of the populations A_0 and A_1 of the two conformational substates 0 and 1 at temperature T is given by

$$A_0 / A_1 = \exp[-\Delta G / RT] \qquad [1]$$

where ΔG is the difference in Gibbs free energy between the two substates,

$$\Delta G = \Delta E + P \Delta V \qquad [2]$$

Here, ΔE, ΔV, and ΔS are the differences in internal energy, volume and entropy between the two substates. Pressures shift the equilibrium ratio by the factor **exp[-PΔV].** Pressure also affects reaction rates: if a reaction B → A occurs in the conformational substate i, the reaction rate coefficient k_{BA} can be written as

$$k_{BA}^{i} = \nu \exp(-G_{BA}^{*} / RT) \qquad [3]$$

where

$$G_{BA}^{*} = E_{BA}^{*} + PV_{BA}^{*} - TS_{BA}^{*} \qquad [4]$$

is the activation Gibbs free energy and ν is the frequency factor in the substate i. The star indicates the Gibbs free energy is ideally measured at constant viscosity. The factor $\exp[-PV^{*}{}_{BA} / RT]$ can either speed up or slow down the reaction rate; i.e. pressure affects chemical equilibria and reaction rates. The following equation yields the reaction volume:

$$V^{*} = -(\frac{RT\partial \ln K}{\partial P}) \rightarrow \frac{\partial \ln K}{\partial P} = -\frac{V^{*}}{RT} \qquad [5]$$

It should be noted that the above explanation for pressure effects on proteins is for the simplest model possible. A protein molecule in a given state does not exist in only one or two conformations, but assumes a large number of conformational substates (CS) [7] which are most likely arranged in a hierarchy.[8] As discussed above for the simplest case of two conformations, pressure can affect protein dynamics and reactions in two ways. Within a given CS, pressure can change reaction rates according to the above equations; the change depends upon the activation volume V^*_{BA} which may be different in different CS. Equally important, however, is that pressure may shift the population from one substate to another. Since the different CS may have different reaction rates, pressure can change the overall reaction rate by a factor that cannot be described by an activation volume alone.[5]

In general, we know that bond formation processes should be accelerated by the application of pressure except in cases where the bond formation is accompanied by major changes in conformation or electrostriction that could possibly counteract this effect.[9] Several studies [10] have reported a positive activation volume for the formation of MbCO, a process that involves bond formation. In contrast, the activation volume of the formation of MbO_2 is negative, which is expected for a bond formation process. In addition, other studies [11] [12] have now clearly indicated that the binding of O_2 and CO involves different activation barriers and rate-determining steps.

Generally, the response of a system to the application of pressure is explained by the principle of Le Chatelier, which states that if a chemical system at equilibrium experiences a change in concentration, temperature, volume, or total pressure, then the equilibrium will shift in order to minimize that change. In the case of a system increasing in pressure, it will reduce its

volume. This reduction in volume can be the consequence of a chemical reaction, a closer packing of the molecules, or where a protein's unoccupied spaces (cavities) in its native state are penetrated by water molecules. It is evident that of all the thermodynamic properties of a system, volume is the easiest to grasp intuitively, and this concept that is well understood at a macroscopic level is now being applied at the molecular level.[13]

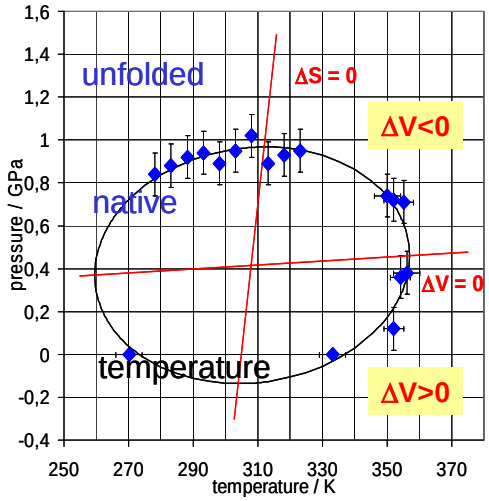

Figure 3: Pressure/Temperature phase diagram [14]

A major advantage of using pressure for performing experiments on proteins as compared to the more conventional approaches of varying the temperature, is that one can separate the effects of density and temperature. The phase diagram in Fig. [3] is of a pressure-temperature plane for the stability of proteins, and can be divided into two regions: native and unfolded states. The protein is stable in its native state inside the ellipse, and ΔV depends on temperature and pressure. As an example, the effect of pressure at several kbar will give an egg white an appearance similar but not identical to that of a cooked egg. At high pressure and high or low temperature, changes are, in most cases, irreversible (plastic or conformational).

A number of physical factors that control the behavior of proteins under pressure are now

becoming clearer: at pressures less than 3kbar, it appears that the compression of protein cavities and an increased hydration is the main effect, and the role of the solvent is providing very useful insights into the dynamics of protein behavior. For example, studies have shown that glycerol decreases the compressibility of the protein interior.[15] These studies also suggest a role for water as a lubricant for the conformational flexibility of proteins. Probing the difference between the pressure, heat and cold denaturation/unfolding is not easily done when considering the possible side effects that result from the unfolding that make a simple analysis somewhat complicated. Heat denatured proteins are extremely prone to aggregation.[18] This may also occur, under certain conditions and with certain proteins, after compression. But whether these effects are protein specific or not remains to be seen. Certain water soluble polymers show pressure-temperature phase diagrams similar to those of proteins, which is also of particular interest.[16] Although the number of pressure studies is limited, it seems that the stabilizing effect against temperature denaturation is also found against pressure denaturation.[17] [18]

2.2 Basics of Raman Spectroscopy

Raman scattering was experimentally demonstrated in 1928 by C.V. Raman.[19] Raman Scattering, or the inelastic scattering of light, from energy excitations in a material gives structural and dynamic information at the molecular level. It reveals the "fingerprint" of the molecule, where the molecular components and functional groups of a material can be seen, which is characteristic of only that particular material. In forensics, for example, identifying the fingerprint region of an unknown material leads to a positive identification of that material. Since the development of the laser almost 40 years ago, a much wider application of Raman

scattering in experimental endeavors has been made possible, and has provided an exceptionally useful tool in the study of biomolecules.[20] The non-destructive nature of the probe, flexibility in sampling arrangements, and a technical revolution [20 21 22 23 24] in multi-channel detection and Rayleigh filters (rejecters of unusable info) have opened up many new areas where Raman measurements have proven to be very informative.[25]

The integration of a microscope in Raman systems adds even more versatility to Raman spectroscopy, providing spatially-resolved compositional information. One simple benefit of this is that where only a very small amount of a sample is available, high quality Raman spectra can be obtained.

In Raman spectroscopy a sample is irradiated with light energy, typically from a laser source. The radiation from the laser, when incident on a system, is mostly scattered without a change in frequency. But there does occur *some scattering* of light with an altered frequency, and this is Raman scattering. There are elastic and inelastic types of scattering: Rayleigh scattering, where the excited molecular system emits photons of the same frequency as the incident laser source; Stokes scattering, where the system emits a photon of lesser energy than the incident laser; and anti-Stokes scattering, where photons of greater energy are emitted. Raman Spectroscopy measures energy increases and decreases in vibrational energy spacing in the ground electronic state of the molecule after being irradiated with the light energy. The excitation of the molecules' vibrational energy, from the laser directed at the sample, reflects that energy through the Raman microscope's system of filters and monochromators and eventually onto a CCD detector which translates the energy into an energy spectrum.

A Raman spectrum is an intensity vs. wavenumber graph that shows the wavenumbers where the vibrational modes in the molecule reside. Vibrational bands (modes) can be measured

in relative wavenumbers to that of the Rayleigh line. Wavenumbers (*inversely* proportional to the wavelength, λ) are used because they are proportional to the energy according to the relation

$$E = \frac{hc}{\lambda} \qquad [6]$$

where h is Plank's constant and c is the speed of light.

Classically, we can explain the basic physics behind Raman scattering. The polarizability of the atomic bond is the variable of a function of the inter-nuclear separation distance, or in other words, the tendency of a charge distribution (or, a molecule) to be distorted by an external electric field. When the electrons of the bond interact with the electric field of the incident energy radiation (the laser), a dipole is generated. The electric field of the incoming electromagnetic wave of the laser is represented by the equation

$$\mathbf{E = E_0 \cos(\omega t)} \qquad [7]$$

where E_o is the amplitude of the incoming wave, and ω is its frequency. To derive the basic features of Raman scattering we can use a *classical approximation*. The induced dipole moment can be written as $\mathbf{P = \alpha E}$, where α is the polarizability tensor. The polarizability of the molecule can be expanded as a Taylor series:

$$\boldsymbol{\alpha = \alpha_0 + \left(\frac{\partial \alpha}{\partial q_k}\right)_0 q_k + \left(\frac{\partial^2 \alpha}{\partial q_k^{\,2}}\right)\frac{q_k^{\,2}}{2} + \ldots} \qquad [8]$$

where α_0 is the polarizability at equilibrium, q is the vibrational displacement (which is the position of the nucleus and the dynamical variable if the excitation is a vibration), and q_k is the displacement of the kth normal coordinate which can be represented by simple harmonic motion as $\mathbf{q_k = q_k^0 \cdot \cos(\omega_m t)}$ for a molecule oscillating at frequency ω_m. We can neglect the higher power

terms and obtain for the induced dipole moment (the polarizability of the molecule, or P) the equation:

$$\mathbf{P = \alpha_0 E_0 \cos(\omega t) + \left(\frac{\partial \alpha}{\partial q_k}\right)_0 E_0 q^0{}_k \cos(\omega t)\cos(\omega_m t)} \quad [9]$$

This can be rearranged with a trigonometric identity, giving:

$$\mathbf{P = \alpha_0 E_0 \cos(\omega t) + \left(\frac{\partial \alpha}{\partial q_k}\right)_0 E_0 q^0{}_k \frac{1}{2}[\cos(\omega + \omega_m)t + \cos(\omega - \omega_m)t]} \quad [10]$$

The first term of Eq. [10] describes the Rayleigh scattering and is proportional to α_0. The second term and third terms concern the frequency shifted light; the anti-Stokes and Stokes Raman scattering, respectively. Both terms are proportional to the partial derivative of α with respect to q. The Raman active modes are determined by the selection rule $\frac{\partial \alpha}{\partial q} \neq 0$, meaning; the molecular polarizability change, or the amount of deformation of the molecule's charge distribution, with respect to the molecule's vibrational displacement, must not be zero in order for the Raman effect to occur.

The wavenumber of the Stokes and anti-Stokes lines are a direct measure of the vibrational energies of the molecule. Stokes and anti-Stokes lines are equidistant from the Rayleigh line (the spectral line which is simply the wavenumber of the laser excitation source), because in either case one vibrational quantum of energy is gained or lost. Anti-Stokes lines are less intense because it only occurs in molecules that are vibrationally excited prior to the excitation. Hence, only the Stokes lines, which are more intense, are measured in Raman spectroscopy. For a vibrational motion to be Raman-active, there must be a change in polarizability of the molecule with the vibrational motion, i.e. the selection rule, which is what

sets Raman apart from Infrared spectroscopy, which says that there must be a change in the molecule's dipole moment during the vibration. In Raman scattering, the vibrations or any other excitations modulate the polarizability tensor, causing the induced electric dipole moment to radiate at different frequencies from the electric field vector of the incoming light wave. [20] A quantum mechanical representation of the Raman effect is shown in Fig. [4].

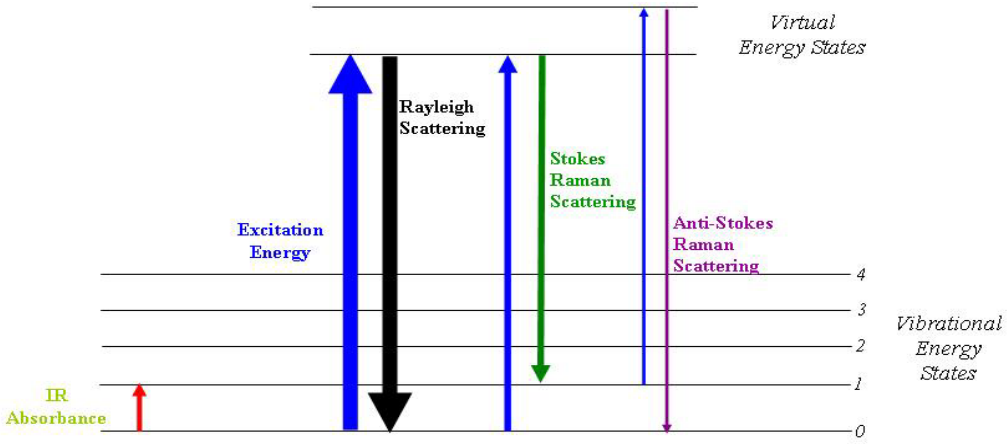

Figure 4: Quantum mechanical representation of the Raman effect

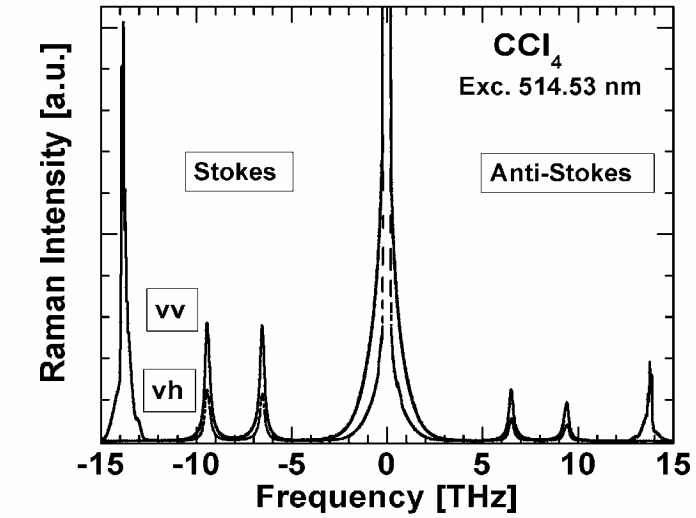

Figure 5: Raman spectra of CCl_4 showing the Stokes and anti-Stokes lines; vv and vh denote polarization of the scattered light parallel and perpendicular to the scattering plane.

Fig. [5] displays the Raman spectrum of CCl_4. From the figure we see that the Stokes

scattering is higher in intensity than the anti-Stokes scattering, and equidistant from the Rayleigh line since they are both separated by one energy state. The Raman shift from the Rayleigh line has to do with the level of vibration. The amount of polarizability change determines the intensity of the peaks. The *difference* in intensity can be explained by the relative intensities of the two types of scattering. The intensity ratio of the Stokes line to anti-Stokes is given by a Boltzmann factor: $\exp(-\frac{\mathrm{h}\omega}{kT})$, where h is Planck's number and k the Boltzmann constant. The Boltzmann factor weighs down molecules which occupy the populated higher energy states.

Anti-Stokes vibrations are observed only at low frequencies. In the figure we can see that at 13.8 THz and -13.8 THz (or $\pm 459\,cm^{-1}$), the Stokes line (-13.8 THz) has a greater intensity than the anti-Stokes line by about a factor of 6. But at frequency shifts just beyond the scale of the figure, the anti-Stokes scattering intensity is about 100 times weaker than the Stokes scattering intensity.

CHAPTER THREE: EXPERIMENTAL SETUP FOR HIGH PRESSURE

In chapter three I will be discussing in detail the high-pressure Raman spectroscopic apparatus that we have built, and which we expect to play an important role in future studies of biomolecular systems and proteins. In sections 3, 4, and 5 of this chapter, I will discuss and provide the complete procedure of preparing a sample for high-pressure analysis. Hence, these latter sections are written in "instructional form".

3.1 Basic Description of the System

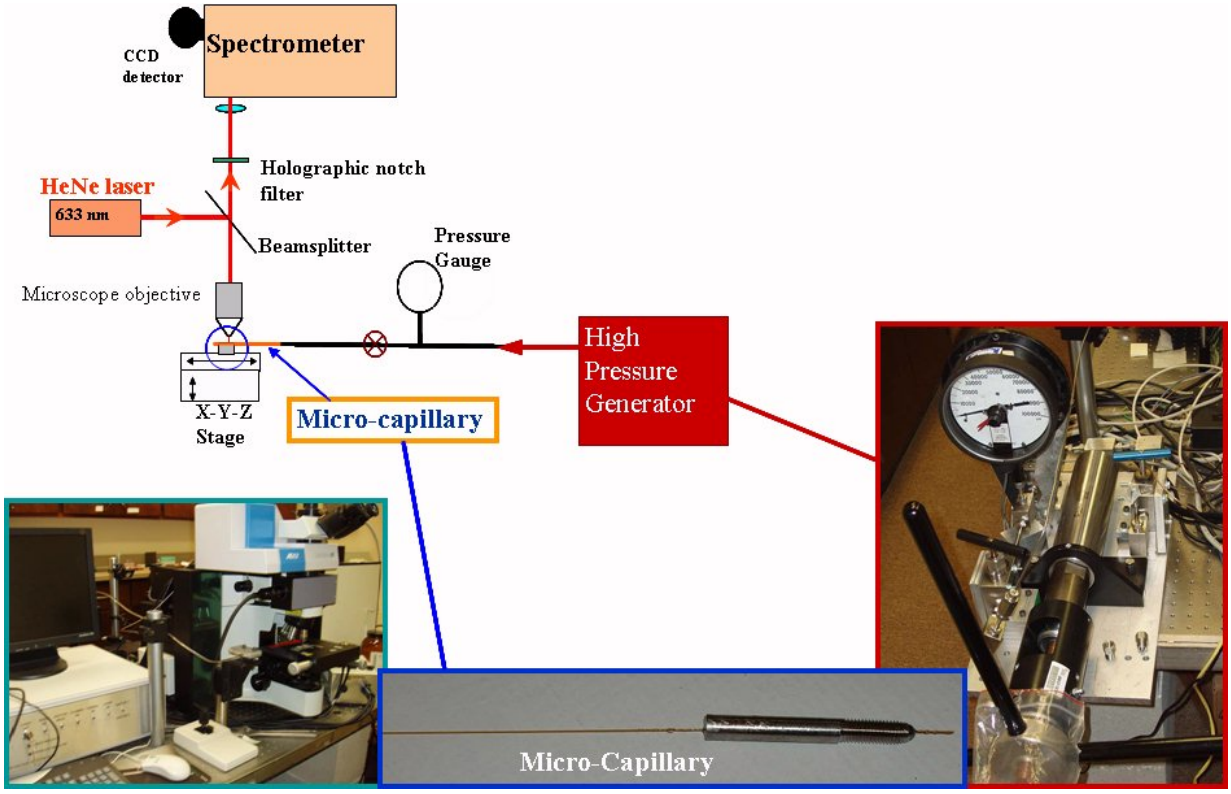

Figure 6: Schematic of high pressure Raman system; a blue circle marks the area where the sampling is done.

An overall view of the high-pressure Raman system is represented in Fig [6]. In basic terms, it has a Raman part and a high-pressure part that are joined together; a high-pressure pump is connected in series to a silicon micro-capillary holding the sample that the Raman system is analyzing. But the series of connections and joints between them, which must be fitted very delicately, is what introduces the careful and meticulous part of its construction.

The entire pressure system must be rigidly fixed in place so that no movement is allowed, since we are dealing with a series of high pressure hose and valve connections that are fitted together to a precision that at ultra high pressures the connections still hold pressure. Any undue movement of the system (bumping it, for example) can cause any one of these connections to falter, and hence, leak, which would result in a failure to pressurize and require a re-adjustment of the whole system.

The Raman Microscope that we use is the LabRam HR800. It is a Raman spectrometer integrated with a confocal system which gives it a 1μm-lateral x 2μm-axial spatial resolution. The laser excitation can be from the visible to near-infrared. The ease of the use of this system, in practical terms, means that a lot of work can be done on this system very time-effectively, not to mention its easy alignment and optical viewing through the scope. A sample can be viewed by an optical video camera, which allows focus on a selected area of the sample. It has a high sensitivity CCD detection system which analyzes the energy information and gives the spectra. Since this is digital, the information can be manipulated in a number of ways, by pixel for example, to maximize the understanding of the spectrum in many ways.

We used two different types of capillary tubing for the high pressure experiments. We used cylindrical capillaries—"Flexible fused Silica Capillary" (model # TSP050375—Polymicro

Technologies)—as well as square-shaped capillaries—"Square flexible fused Silica Capillary" (model # WWP050375—Polymicro Technologies).

3.2 Photos of Experimental Equipment

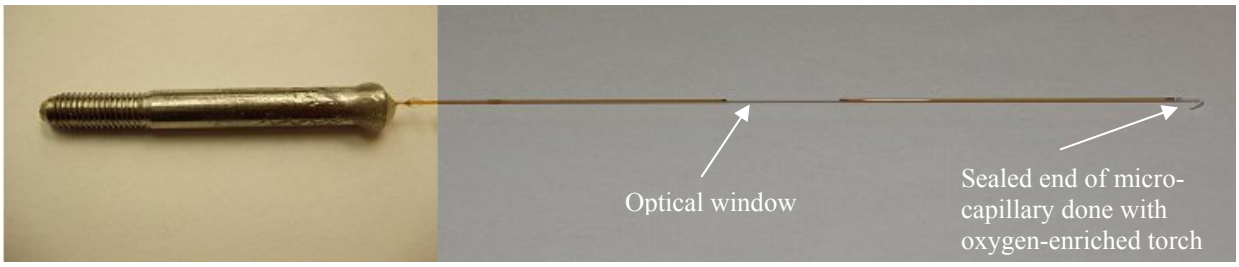

Figure 7: Micro-capillary pressure cell; threaded pressure tubing glued to micro-capillary

Figure 8: High pressure generator; liquid medium, hand-operated

Figure 9: Front view of confocal Raman system and computer setup for control of system (viewing spectral data, camera viewing through microscope, and control of spectroscopy software)

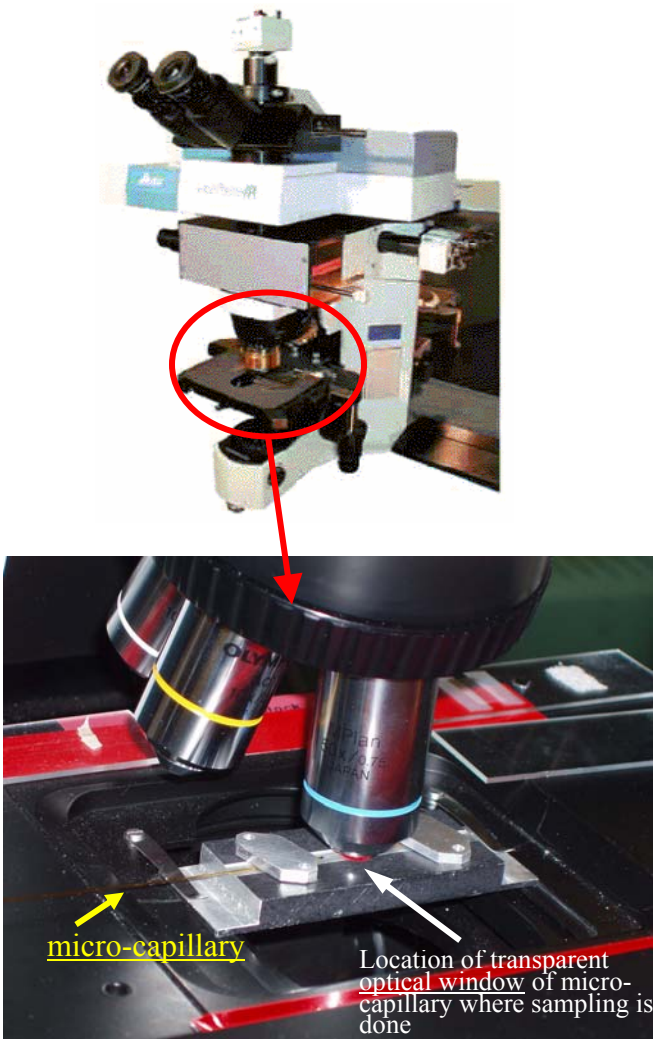

Figure 10: Front view of confocal Raman system with close-up of microscope stage

3.3 Construction and Details of the High-Pressure System

Initial tests were conducted with a compressor using nitrogen gas as the pressurizing medium. After acquiring a new pressure pump, I began constructing a new high-pressure apparatus that would greatly simplify the operation and increase the pressure range of our experiments, much in contrast to the previous high-pressure systems that we had already tried. The new hand-operated pump that we had acquired was the ideal high-pressure pump for our needs (maximum pressure output, liquid medium and greatly simplified operation).

The pump is fastened to the optics table on which rests the Raman microscope and spectrometer, minimizing the risk of the adjoining pressure tubing from undue movement and connection breakage. The pump's output connects to a fastened 1/8" diameter high pressure tube, which is long and can bend as desired, which reaches across the optics table and arrives at a short working distance from the microscope objective. The end of this 1/8" high pressure tubing is where we make the connection with micro-capillary, which rests directly under the microscope objective. This works by connecting the capillary to a pressure plug, which is connected to the pressure tubing that comes from the high pressure generator. A metallic coupling unit fits the pressure plug, and this "provides the high pressure connection between the capillary and the pressure tubing." [3] There is a specially made substrate onto which we place the micro-capillary. It is made of aluminum plating and was machined especially for this experiment, with a 1/32" groove cutout where the capillary sits. It has the same dimensions as regular glass substrates, but is about ¼" thick, and is painted black so as to reduce reflection from the shiny aluminum surface. It has a hole drilled through it so that the laser can pass through the capillary unimpeded by any surface beneath it. At first, we were using standard glass substrates, and the reflection of the glass substrate was causing a lot of background fluorescence in the spectra. Using fused

silica capillaries significantly reduced the fluorescence. During the experiment, we fasten the capillary down by two small pieces of aluminum to prevent the capillary from moving, which is important since the focus point of the laser beam must stay within the hollow 50μm inner diameter of the capillary. These small weights are put into place before focusing.

Preparation of the micro-capillary is simple in theory but in practice requires a lot of care. We connect the silicon micro-capillary to the steel high-pressure tubing by gluing them together with a two-part epoxy. The glue also needs to withstand the high pressure, and it will if prepared exactly right. There are a number of factors in the gluing process that are critical to preparing it correctly, which we were able to determine over a lengthy period of time by trial and error. The exact gluing process is critical and is provided in detail in the appendix section.

3.4 Capillary Preparation

First, a piece of the capillary is cut to the desired length that will reach the microscope objective from where it connects to the pressure system's output (the length of the capillary, in our case, requires about a ten inch piece). It is then glued into a 3" piece of high-pressure steel tubing, which is threaded at one end. By connecting this threaded piece of steel tubing to the steel *output tubing* of the pressure pump, the silicon capillary is able to be pressurized. Once the capillary is glued to the steel connector piece, it must be tested to ensure that there is no blockage in the capillary that would prevent the transmission of pressure. To do this, we simply connect it to a pressurized air source and feel if air comes through the end of the capillary. Once that is done, a small "window" must be made in the capillary; the capillaries come from the manufacturer with a gold-colored polymide coating that completely covers the capillary. To

make the optical window, you must strip off a small section of this coating to get to the silica surface, which is clear and transparent; the length of the section being roughly one inch. This optical window area of the micro-capillary is where the Raman microscope's laser will pass through the transparent silica to focus on the sample inside the micro-capillary. The optical window rests directly beneath the microscope objective, which focuses the laser onto the sample. The window is made very easily by applying an open flame directly to the coating, which burns it off. The flame is applied until the gold-colored coating becomes charred black, which takes only a few seconds to occur. The charred polymide coating can then be wiped away using an ethanol-soaked tissue such as a chemwipe, which will then reveal a clear silica "window". The process is repeated (open flame, then ethanol) if some of the charred coating cannot be removed with the ethanol the first time. But some care is required in this step since the resulting silica will be brittle compared to the strength of the polymide coating, which gives the coated capillary tremendous flexibility. Since the imaging will be done at the optical window, do not handle or touch this area. This is because oil residue from fingerprints is very fluorescent, which will add background fluorescence and negatively affect the data. Hence, the capillary should only be handled at the ends.

To know exactly where to make the capillary's optical window, put the capillary into position on the microscope stage, as it would normally be installed for a real experiment. Mark the spot on the micro-capillary that lies directly under the microscope's objective using a permanent black marker, then apply the open flame at that location of the micro-capillary to burn off the coating.

At this point the organic sample is ready to be loaded into the capillary. A number of different techniques can be used to draw the sample into the capillary's 50μm-diameter hollowed-out inner bore. Which method to use depends of the viscosity of the liquid sample. For low-viscosity samples, merely applying suction with a syringe attached to the threaded end of the capillary will draw the liquid sample from it's container into the capillary. For higher viscosity samples, a vacuum pump attached in like manner is required. To be sure that the sample is inside the capillary, we take a quick, preliminary Raman spectrum, with no applied pressure, and look for the characteristic peaks of the sample to confirm its presence. Once it is determined that the sample is indeed inside the capillary, the free end of the capillary must be closed off to seal the opening, so as to hold the pressure. When this is done the experiment is ready to proceed. Sealing the end of the capillary is done by melting it. This can only be done using an oxygen enriched flame of a blowtorch, as only a high temperature flame will be able to melt the highly heat-resistant silica (the melting point of silica is roughly 3000° F). All that is required is to touch the extreme end of the capillary with the flame until you can visibly see the end melt. This takes no more than a couple seconds. Since the thermal conductivity of silica is very low, heat will not be readily transferred to the bio-sample or damage the sample, provided that a large enough space exists between the melted end of the capillary and the sample itself (where the optical window is). We normally cut the capillaries to a length that leaves us around 2 or more inches of buffer space between the two points. Two important factors to the melting/sealing procedure are: a) to make sure that no air bubbles form in the melted silicon, as the air bubbles are prone to burst under high pressure; and b) to melt a seal that angles downward, to be acute relative to the rest of the capillary. At this point the capillary is ready to be loaded and pressurized to take high pressure spectral data of the sample. Once the capillary is

loaded into place and screwed into the pump's output nozzle, the next step is to focus the laser on the sample, which is done by focusing the microscope objective on the capillary's inner bore. It's best to first use a lower power objective to focus on the capillary since it's a much easier

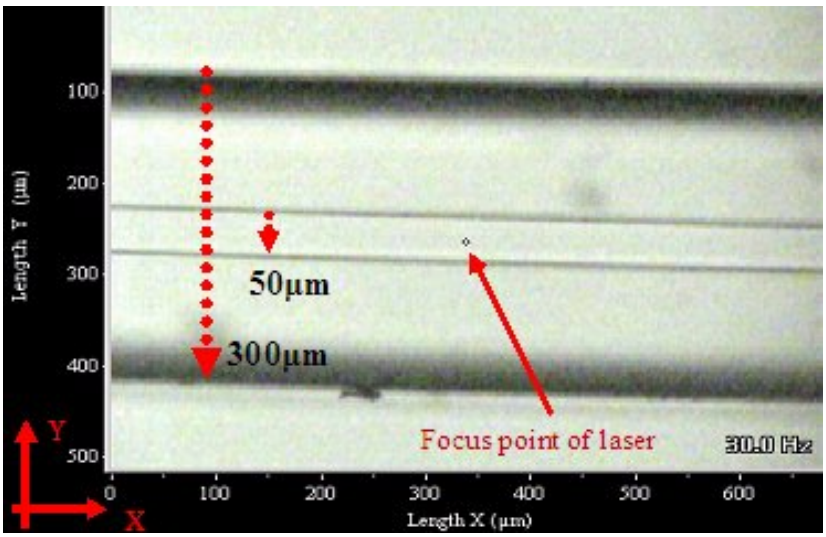

Figure 11: Optical view of the micro-capillary as seen through the microscope camera

way to find the location. Fig. [11] shows a picture of the capillary as seen through the microscope objective and the system's optical camera. Focusing the laser on the sample is done by optically placing the laser's focus point inside the capillary's inner diameter. This is done by first getting the inner walls of the capillary into focus. This alone will center the Z-direction to the exact center depth of the capillary cylinder, since the focus point lies in the same plane as the optically focused wall boundaries. Then, center the Y-direction of the inner diameter on the laser's focus point. Once the laser is centered properly in the Y and Z directions (focused on the inner diameter), we can switch to the higher power objectives for a more precise acquisition of data. Since our other microscope objectives are aligned to the same center, switching to another objective will require only slight adjustments in Y and Z to further refine the position. If, after

switching to higher power objectives, the location of the inner diameter of the capillary is still uncertain with the optical view, it can be found by looking for wall boundaries that are 50μm apart, using the calibrated size scale on the camera image.

Gluing the micro-capillary into the threaded high pressure piece of tubing is an important step. After all, this seal of glue must withstand high pressures. We use a two-component epoxy, which is of the *slow curing type*, requiring 12 hours to completely cure. Initially, we frequently encountered problems with leaks using this epoxy; at around 1.5 kbar the epoxy seal would typically break. However, this epoxy has a strength rating that increases with an increased temperature environment; additionally, the curing time is greatly reduced when exposed to higher temperatures. When cured at around 180°C, the strength of the epoxy increases 5-fold, to a point where the seal does not break under high pressure (provided the other aspects of the gluing procedure are done correctly). After a long period of trial and error, we were finally able to come up with a gluing procedure that works 70% of the time; meaning that 70% of the capillary pressure cells we prepare work and hold pressure throughout the experiment at the pressures we choose (up to 4.5 kbar). At lower pressures up to 2.5 kbar, the success of the capillary pressure cells in holding the pressure is nearly 100%. However, there is one relevant thing to note; if the threaded steel tubing were to have a smaller inner-diameter, just large enough to fit the micro-capillary into, the epoxy seal would probably hold pressures > 3 kbar more easily than with the factory made steel tubing that we use, whose inner-diameter of .08" is relatively much larger than the 350μm diameter of the micro-capillary. The complete procedure of gluing the micro-capillaries is included in the appendix of this thesis.

3.5 Other considerations regarding the Micro-capillaries

One late development regarding the pressure stress on the optical window portion of the micro-capillaries is that they were *sometimes* breaking at high pressures. I tried a couple different approaches in an attempt to determine the problem causing the breakage, which was difficult to understand since the manufacturer has the capillaries rated at 100,000PSI (≈7Kbar). This most surely has to do with the variability in the process of making the optical window; variations such as the amount of time that the flame is exposed to the capillary. If this remains a problem in the future, there are other ways of stripping the polymide coating from the capillaries without taking away as much strength of the glass that the open flame seems to do. In fact, it is explicitly stated by the manufacturer that an open flame as well as regular propane torches will make the glass "brittle". So, in implementing some of the other methods of stripping off the polymide coating, the structural integrity of the capillary's optical window glass, while under high pressure, will be preserved. These other methods of stripping off the polymide coating include baking at high temperatures or removal by laser. The details of these alternative methods are available on the website of the capillary's manufacturer, Polymicro Technologies.

In the early phase of our project, we decided to try the square micro-capillaries rather than the cylindrical micro-capillaries since the results that we acquired beforehand were good. For example, the intensity of the OH stretch for water seen in the square capillaries had a higher intensity than that seen in the cylindrical capillaries, by almost a factor of two. This is certainly because the laser was passing through a flat surface rather than a curved one. We have since abandoned using the square capillaries primarily because of the maximum pressure rating issue, as the cylindrical capillaries have proven to have high pressure integrity.

CHAPTER FOUR: RESULTS AND DISCUSSION

In this chapter I will present fluorescence and Raman spectra at variable pressure. For fluorescence experiments we choose fluorescein. From the fluorescein data we were able to measure a pressure-induced shift in the fluorescence spectrum. Raman spectra on amino acid and protein solutions will then be presented.

4.1 Spectral shift of fluorescein with pressure

The process of fluorescence differs from Raman effect in that, in the case of fluorescence, the incident radiation is absorbed completely by the molecules and the molecular system is transferred to an excited state from which it can go to various lower energy states after a certain lifetime. The primary difference between the two is that the Raman effect can take place for any frequency of incident radiation; whereas for fluorescence, the excitation must be in an absorption band, and the fluorescence emission is shifted towards the red (Stokes shift).

We measured the fluorescence of fluorescein, and demonstrated that small pressure-induced spectral shifts can be resolved with our setup. Fluorescence spectra of fluorescein were measured at various pressures, from ambient pressure up to 2 kbar, at 10 second sampling times, using both the 100 and 600 groove/mm diffraction gratings. We used a blue 488 nm argon-ion laser for the radiation source. Our reason to sample the fluorescein with the two different diffraction gratings was simply to see a consistency between the two sets of results. Since the spectral shift is very small, we wanted to verify one set of results with another independent set of results. The data from both sets indeed support one another and verify the results.

Fig. [12] shows the spectra of fluorescein at various pressures. The series of curves are color coded according to the pressure levels in the figure's table. The pressure table represents the order in which we pressurized the system, in steps, up to 2Kbar, and as we depressurized back towards ambient pressure. The decrease in intensity in the various spectra in Fig. [12] may be attributed to the photobleaching of the fluorophores.

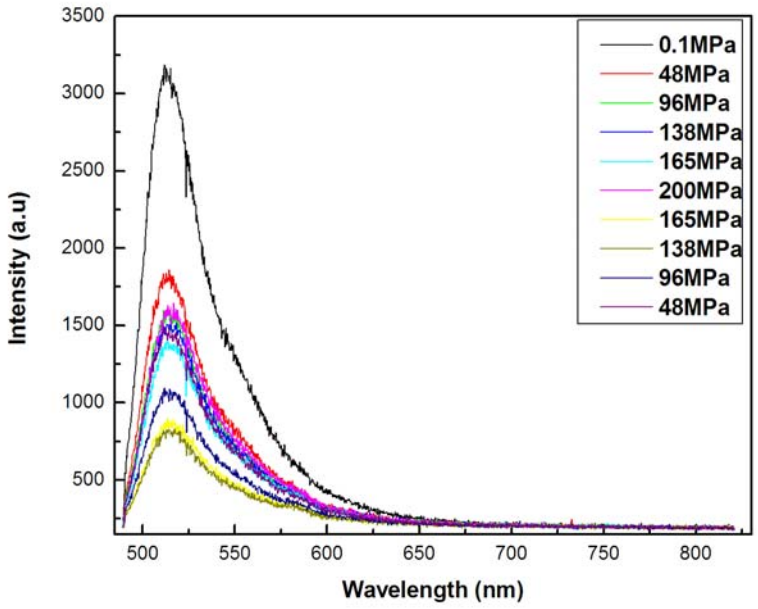

Figure 12: Spectra of fluorescein at various pressure levels

The peak maximum shifts in wavelength as the result of the effects of pressure induced on the fluorescein molecules. However, fluorescein is not an organic material, so the vibrational shift is not attributed to a pressure induced conformational change, as would be the case in proteins and amino acids. The shift in this case may be attributed to a change in the solvent interaction. Fig. [13] shows one example graph of the data fitting done to the spectra at all recorded pressure steps. An analytical expression was used to fit the data using the Origin

Software that we use for spectral analysis. Fig. [14] shows the results of the data fitting of spectra taken at different pressures, showing an increasing wavenumber shift with increasing pressure. One important aspect of the pressure vs. wavenumber graph of Fig. [14] is the way in which we measured the pressure changes. The pressure was increased in steps and a measurement was taken at each pressure level. After measuring at 2 kbar, we reduced the pressure and took measurements at the same pressure levels

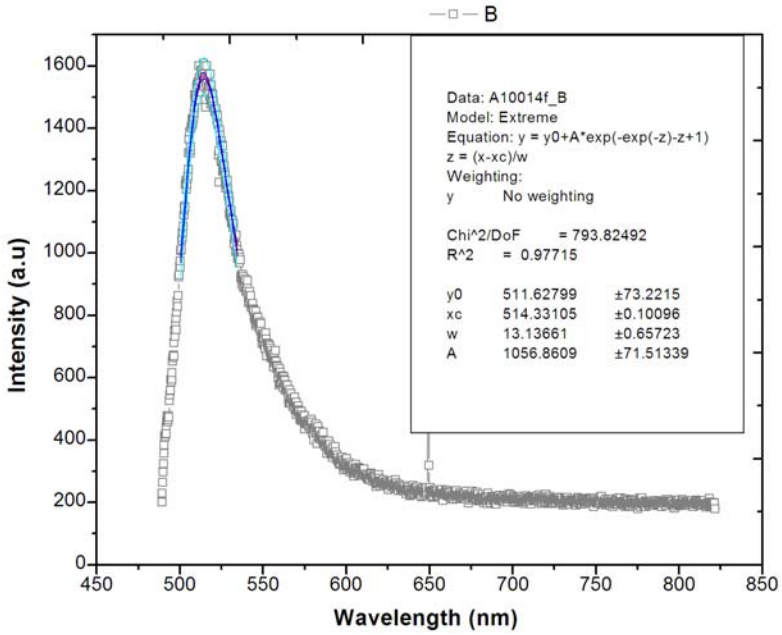

Figure 13: Curve fitted in the peak region to locate the maximum accurately; lower resolution spectra

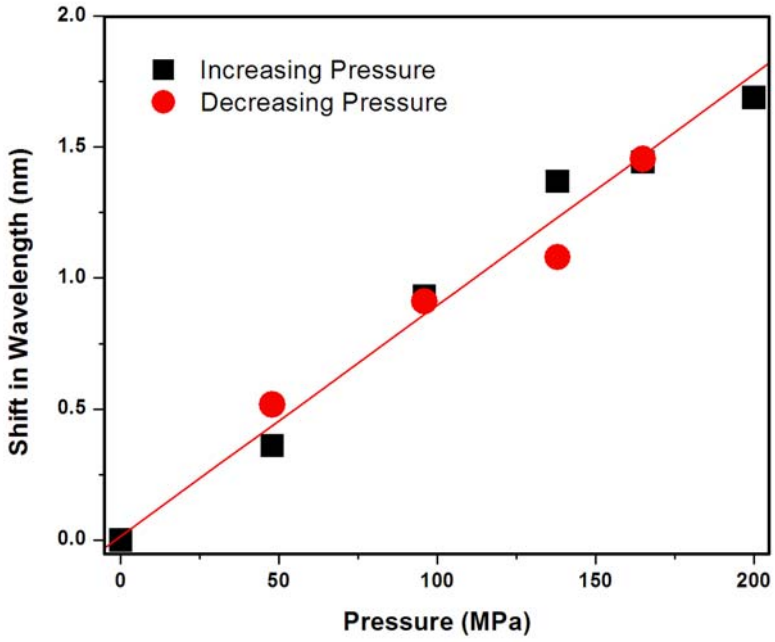

Figure 14: Results of data fitting showing spectral shift in wavelength vs. pressure

as we de-pressurized the fluorescein back to ambient pressure. The black square dots in Fig. [14] represent the pressure levels as we increased the pressure, and the red dots represent the pressure levels as we decreased the pressure. As can be seen from the figure, the peak positions in both cases match. This shows the stability and accuracy of the system.

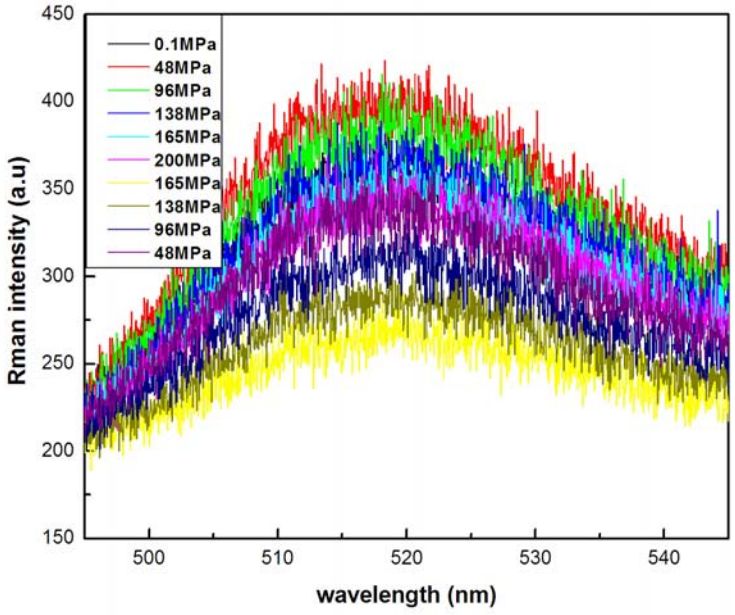

Figure 15: High resolution spectra of fluorescein at various pressures

Fig. [15] shows the higher resolution spectra of fluorescein at various pressure levels. These spectra were collected with the 600 groove/mm diffraction grating, hence, only the top part of the curve (the peak) seen in Fig. [12] is shown. But that is not a factor since the shift is detected in the peak. Again, the series of curves are color coded according to the pressure table in the figure. To resolve the pressure induced shift, a curve was fitted to the peak in the spectral data. Fig. [16] shows an example graph of the data fitting; the larger number of data points compared with Fig. [13] is due to the higher resolution 600 groove diffraction grating used here. Fig. [17] depicts the results of the data fitting of spectra taken at different pressures, again showing an increase of wavenumber shift with increasing pressure and a return to the molecules' original wavenumbers as the pressure decreases. The shift in Fig. [14] is approximately 1.6nm/200MPa, and the shift in Fig. [17] is approximately 1.4nm/200MPa; a difference of

0.2nm, falling well within the error that the different resolutions of the two diffraction gratings account for (resolution of the 100 groove grating is 0.5nm, resolution of the 600 groove grating is .08nm). The fluorescein is coupled to the solvent. Pressure may cause rearrangement of the solvent molecules around the fluorophore, making the environment more polar. This is consistent with a redshift. The results from both data sets independently verify that a reversible, pressure induced spectral shift was observed in the fluorescence spectra of fluorescein in a micro-capillary pressure cell.

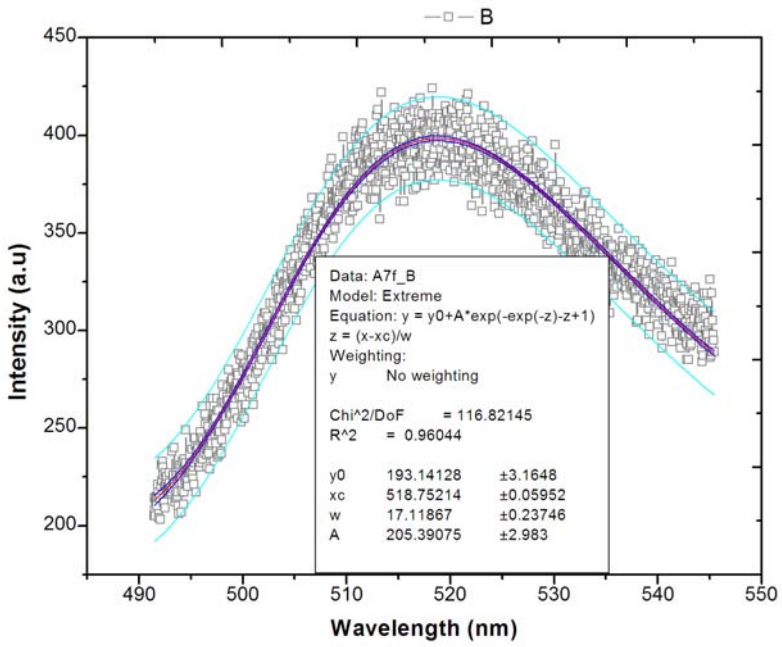

Figure 16: Curve fitted in the peak region to locate the maximum accurately; high resolution diffraction grating

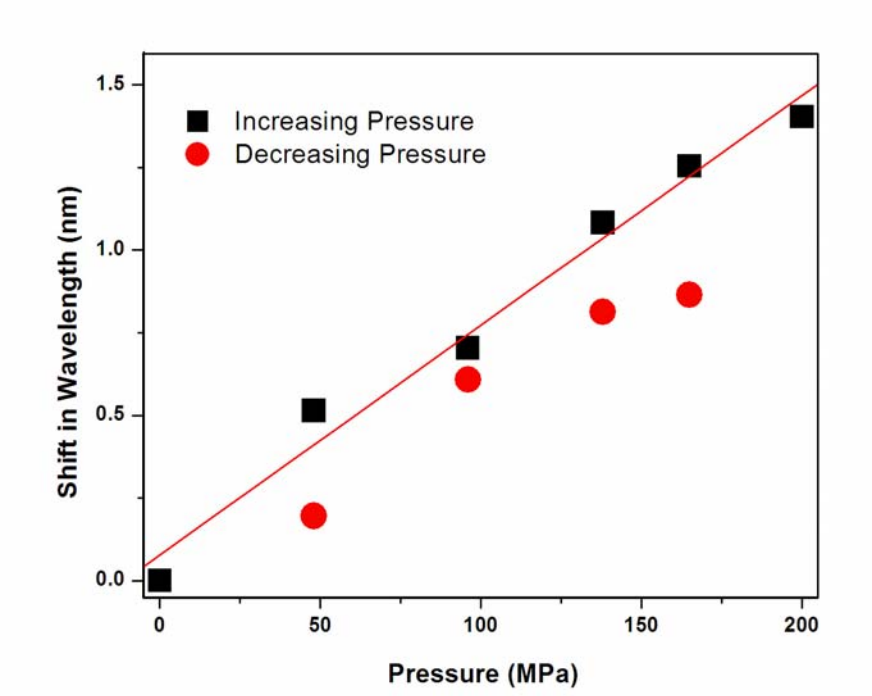

Figure 17: Results of data fitting showing spectral shift vs. pressure; higher resolution

4.2 High pressure Raman spectroscopy with the micro-capillary cell

4.2.1 Spectra of Water

Raman spectra for water are shown in Figs. [18] and [19]. The difference between the two are the sampling times, where the 10 second sampling is much cleaner and has a higher intensity. These first results of water showed us in the early stage of this project that high quality data can be taken from within a micro-capillary. In accumulating spectra of water, we also found that there were a couple factors that led to unwanted background fluorescence, namely, handling the capillaries in a way that deposited oils on the optical window. Thus, careful handling of the capillaries to prevent contamination from, e.g., fingerprints, is very important.

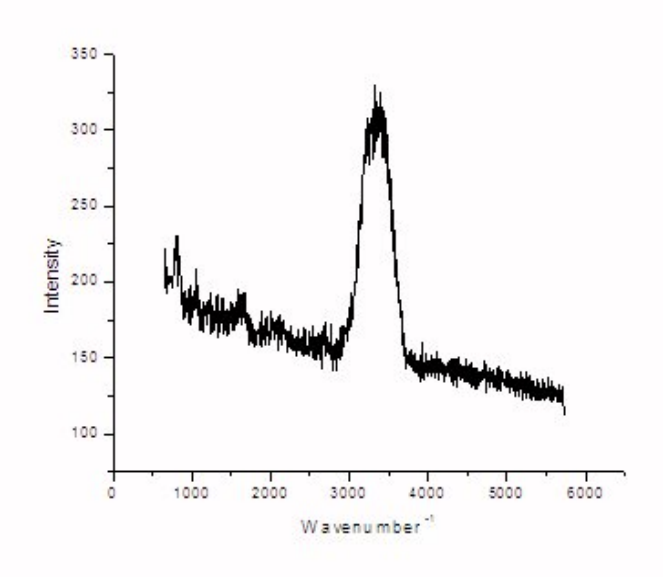

Figure 18: Raman spectra of water; 1 second integration time

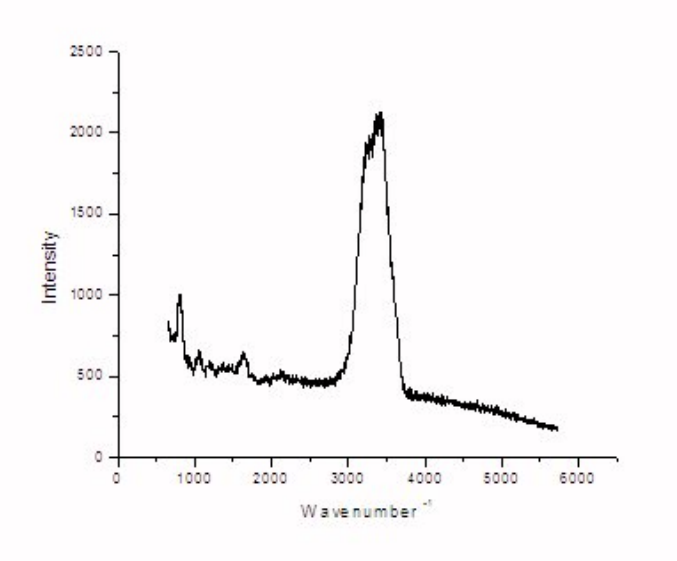

Figure 19: Raman spectra of water; 10 second integration time

4.2.2 Spectra of amino acids

To assess the signal level from biochemical compounds, we applied high pressure to amino acid solutions inside the capillaries and collected Raman spectra. Spectra of two amino

acids, L-Cysteine and L-Alanine, were taken while using a generator using gas as a pressurizing medium, and using the lower-resolution 100-groove diffraction grating. Due to the low resolution of this grating, we were not able to see the pressure induced vibrational shifts in the molecules. However, the data demonstrated that high quality Raman data are obtained with our high-pressure apparatus and setup.

Fig. [20] shows Raman spectra of amino acid solutions L-Alanine and L-Cysteine (1 M), inside a micro-capillary, at both ambient pressure and at a pressure of 1.44 Kbar. In Fig. [20], the amino acids' characteristic peaks are seen in the small, but distinct, peaks at approximately 1400 wavenumbers. This is the C=O stretch of the carboxyl group in the amino acid, otherwise known as the "fingerprint" region; a region of the spectrum that is singular to a particular sample or material. The broad peak at around 3300 wavenumbers is the O=H stretch, or the peak of water, which we dissolved the amino acid into. One distinctive characteristic of the Cysteine spectrum, when comparing to the Alanine spectrum, is the peak that appears at approximately 2600 wavenumbers. This is the thiol group, seen in the figure as the S-H compound, which cysteine contains. Scattering from the silica micro-capillary is seen in the far left side of the spectra, in the region below about 1000 wavenumbers and less, and does not interfere with the spectral data of the sample. The data acquisition time is 100 seconds, using a 633 HeNe laser with a power of 8 mW, at an amino acid concentration of 1 M. Fig. [21] shows the "fingerprint" regions of the amino acid L-Alanine in higher resolution.

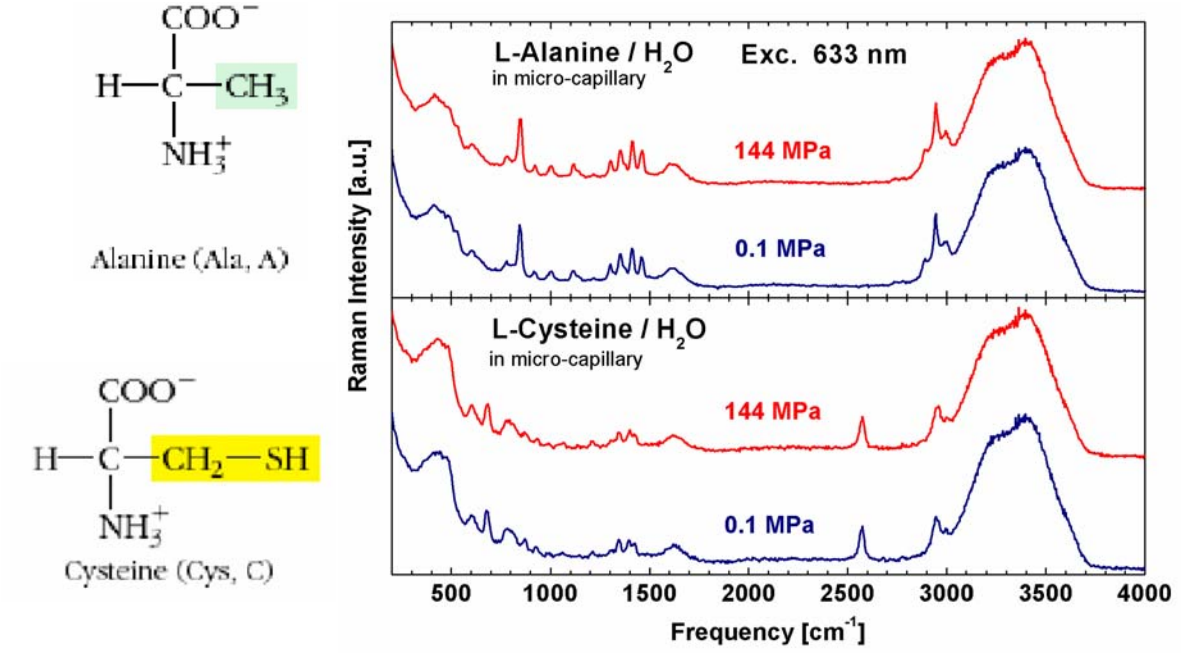

Figure 20: Raman spectra of amino acids L-Alanine and L-Cystein in micro-capillary at both ambient and high pressures

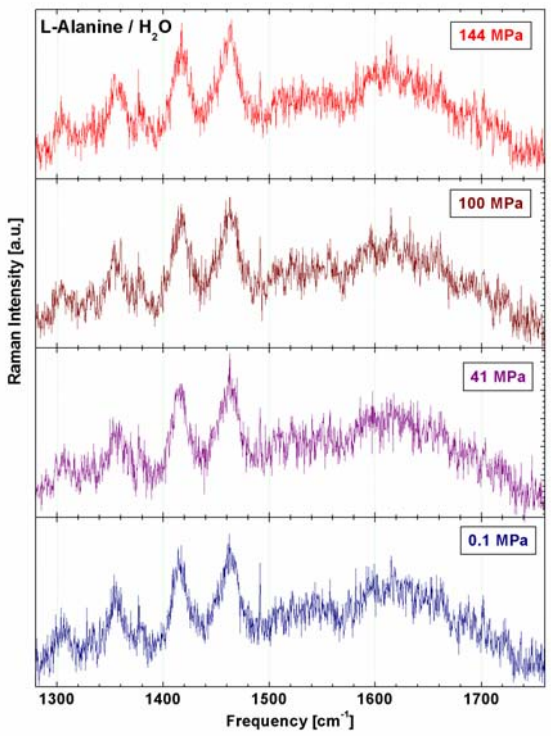

Figure 21: The fingerprint region of L-Alanine in micro-capillary at ambient and various high pressures

4.2.3 Raman spectra of the protein Lysozyme

Fig. [22] shows the Raman spectra of the protein Lysozyme in aqueous solution (15mM) taken inside a micro-capillary at ambient pressure, at 62 MPa, and 141 MPa (ambient, .62 Kbar, 1.4 Kbar, respectively). The data acquisition time is 100 seconds, using a 633 HeNe laser with a power of 8 mW, at a protein concentration of 15 mM. The band positions are characteristic for the native protein, and they have been assigned in the literature. [26] There are relatively sharp lines due to constituent amino acids with aromatic side groups, such as the indole-ring vibrations of tryptophan near 760 and 1012 cm^{-1}. The bands near 1260 cm^{-1} (amide III) and 1660 cm^{-1} (amide I) correspond to frequencies of the peptide CONH groups. Their vibrations are sensitive to protein conformation and are indicative for the native state. A broad band due to the OH-stretch vibrations of water is visible in the region between 3100 and 3600 cm^{-1}.

Due to the low-resolution of 100 groove diffraction grating, we were not able to resolve the pressure induced vibrational shifts in the lysozyme spectrum. The data, however, demonstrates that Raman spectra in the micro-capillary cell can be measured with high signal-to-noise ratio. In the meantime we have addressed this issue by going to a higher resolution 600 groove grating.

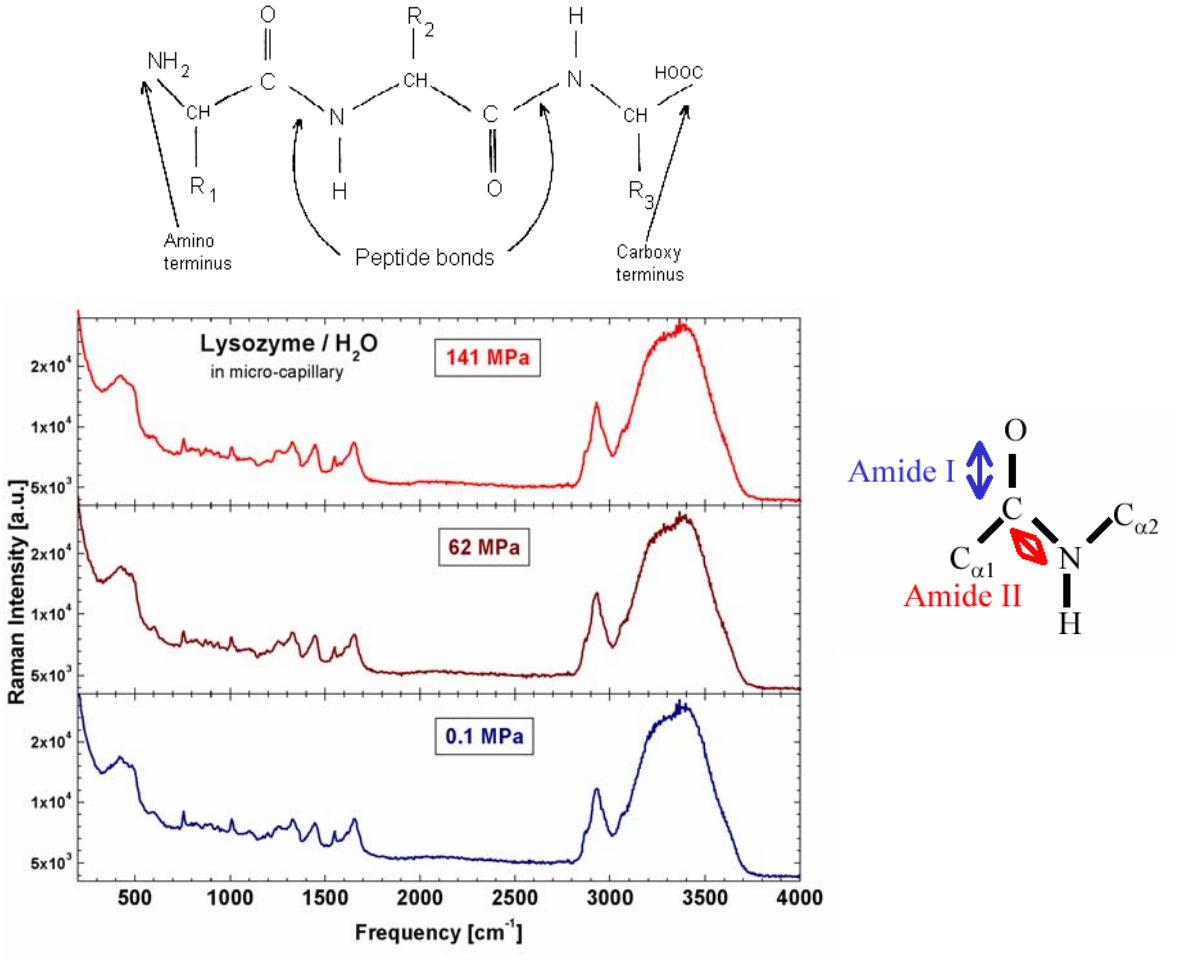

Figure 22: Raman spectrum of Lysozyme in micro-capillary at ambient and high pressures. A depiction of a polypeptide chain showing the peptide bonds, and a figure of the resulting amides, is provided for reference.

CHAPTER FIVE: SUMMARY AND OUTLOOK

Our early experiments proved that high-quality Raman spectra can be taken from inside a micro-capillary, and showed that low intensity Raman signals of organic materials can be detected from within the micro-capillary pressure cell as well. From here there are many potential high-pressure experiments that can be performed. High pressure is an important component to probing conformational changes in protein in the study of protein folding, in that the conformational states of proteins are affected under high pressure conditions. For Raman experiments using excitation under a microscope whose objectives have a high numerical aperture, requiring short working distances of less than one millimeter, the micro-capillary as a pressure cell is very suitable, for biological compounds as well as for fluorescence. Under conditions where samples are minuscule in volume, of a few nano-liters for example, the micro-capillary pressure cell is ideal. There is also a potential for in-situ studies of protein-membrane complexes and individual cells.

APPENDIX: GLUING PROCEDURE IN DETAIL

Preheat a standard laboratory hot plate to a temperature of around 100º C. Soak the 3" threaded steel pieces in a sonicator with acetone. Allowing 5 minutes in the sonicator is sufficient to remove the grease and oil residue inside the steel tubing that will affect the bonding of the glue to the steel. Once removed from the acetone, place the 3" threaded piece of high-pressure tubing on the hot plate and let it remain there while the other preparations are under way. The glue must be liquefied with high temperature before applying for 2 important reasons; a) its viscosity must be greatly reduced in order to get the glue continuously through the hollow of the steel tubing, and uniformly through the steel tubing (it is best to try to fill in as much glue as possible, as this will guarantee a stronger seal); and b) to greatly increase the glue's strength as it cures, which exposing it to a higher temperature will do. This is also done at a temperature of 100º C, and so this can be done on the same hot plate. A small piece of scrap aluminum plating (cleaned first with ethanol) placed on the hot plate is where you deposit the glue to liquefy. At 100º C it takes about 10 seconds for the glue to liquefy, and from there you must act quickly as the high temperature greatly reduces the curing time of the glue (this two-part epoxy glue is mixed with a ratio of 1:1). The 100º C temperature is just right, since higher temperatures will cause the glue to form gas bubbles, which will weaken the glue's bonding strength. Higher temperatures will also cause the glue to cure too fast for this procedure. With the glue liquefied and ready to apply, pick up the 3" threaded piece of steel tubing from the hot plate with a pair of pliers (since it is now very hot), or better, a wooden clothes pin since the metallic pliers will conduct heat and take away some of its thermal energy. With the piece of tubing held upright, apply the liquefied glue to the top of it, and wait while each application of glue sinks down into the hollow of the tubing. Once it sinks, apply more glue. Do this until the glue begins to appear at the other end. At this point, insert the 10" piece

of capillary into the hollow of the tubing and apply more glue to the top of the piece. The goal here is to get the glue as uniformly distributed throughout the hollow of the tubing as possible. There are two specific techniques that we employ to do this, and we do them in succession to one another. The first thing to do, while the glue is still relatively fluid, is to oscillate the capillary up and down with one hand while holding the tubing, with the pliers or wooden clothespin, with the other hand. This helps distribute the glue throughout the hollow part. Doing this with each application of the glue also helps the glue sink into place and settle. The next step is to lay the tubing, now with the capillary attached, on the hotplate on its side and roll the cylindrical tubing back and forth until the glue no longer exhibits fluidity. This further distributes the glue more uniformly throughout. The temperature of the hotplate during this step can be increased to up to 200º C to allow a quicker, and stronger, curing of the glue. Keep about a ½" piece of capillary sticking out of the threaded end so that, once the glue is dry, you can cleave that piece off. This is to ensure that that end of the capillary isn't clogged with any glue from the gluing procedure. We have found that allowing the glue to form a slight cone-shape that protrudes from the end of the threaded end greatly increases the pressure-holding ability of the capillary. This is probably because it doesn't allow the pressurized liquid from even entering the hollow of the tubing.

The 3" pieces of steel tubing can be ordered from the High Pressure Equipment company pre-made and threaded, but we make so many pieces that we order the ¼" diameter tubing in 3-foot long sections and then cut, cone, and thread our pieces from that long bulk tubing. We use the standard coning tool to cone one end of the piece, and a left-handed threading die to thread them, as different high-pressure parts are either left or right-handed threads. This is to prevent the loosening of one inner-connection while tightening an outer-connection. Hence, the

opposing directions of the tightening prevent loosening of the inner-connection. The threading process is begun on a lathe to ensure a near-perfect thread perpendicular to the length of the tubing, after which the rest of the threading can be finished with a die using a hand threading tool. We have also found that cutting out an inverted cone-shaped area on the other end of the steel tubing is helpful for gluing purposes; the downward angle causes the glue to collect in the center, where the entrance to the hollow chamber of the tubing is, and better allows the glue to seep down into the inner-bore of the tubing.

REFERENCES

[1] J.D. Isaacs, R. A. Schwartzlose, Sci. Am. 4, 84 (1975)

[2] G. Weber, High Pressure Chemistry and Biochemistry, NATO ASI Ser., Ser C. No. 197 (1987)

[3] J. Mueller, E. Gratton, High pressure fluorescence correlation spectroscopy, Biophysical Journal 85, 2711 – 2719 (2003)

[4] Day C, Mechanical force may determine the final size of tissues, Physics Today 60, 20 (2007)

[5] H. Frauenfelder, N. Alberding, A. Ansari, D. Braunstein, B. R. Cowen, M. K. Hong, I. E. T. Iben, J. B. Johnson, S. Luck, J. R. Mourant, P. Ormos, L. Reinisch, R. Scholl, A. Schulte, E. Shyamsunder, L. B. Sorensen, P. J. Steinbach, A. H. Xie, R. D. Young, K. T. Yue, Proteins and pressure. J. Phys. Chem. 94, 1024-1037 (1990)

[6] G. Weber, H. G. Drickamer, The effect of high pressure upon proteins and other biomolecules. Quart. Rev. Biophys. 16, 89-112 (1983)

[7] H. Fraunfelder, F. Parak, R.D. Young, Ann. Rev. Biophys. Biophys. Chem. 17, 451 (1988)

[8] A. Ansari, J.B. Berendzen, D. Braunstein, H. Frauenfelder, I.E.T. Iben, T.B. Sauke, E. Shyamsunder, R.D. Young, Proc. Natl. Acad. Sci. U.S.A. 82, 5000 (1985)

[9] H.-D. Projahn, C. Dreher, R. van Eldik, Effect of pressure on the formation and deoxygenation kinetics of oxymyoglobin. Mechanistic information from a volume profile analysis, J. Am. Chem. Soc. 112, 17 (1990)

[10] B.B. Hasinoff, Biochemistry 13, 3111 (1974)

[11] Q.H. Gibson, J.S. Olson, R.E. McKinnie, R.J. Rohlfs, J. Riol. Chem. 261, 10288 (1986)

[12] R.J. Rohlfs, J.S. Olson, Q.H. Gibson, J. Biol. Chem. 263, 1803 (1988)

[13] K. Heremans, High pressure effects on proteins and other biomolecules, Annu Rev Biophys Bioeng. 1982; 11:1-21.

[14] W. Doster, J. Friedrich, Pressure-temperature phase diagram of proteins. Handbook of protein folding, p. 99-124, Eds. J. Buchner, T. Kiefhaber, Wiley (2006)

[15] A. Priev, A. Almagor, S. Yedgar, B. Gavish, Glycerol decreases the volume and compressibility of protein interior,Biochemistry 35 (1996) 2061-2066.

[16] S. Kunugi, K. Takano, N. Tanaka, K. Suwa, M. Akashi, E¡ects of pressure on the behavior of the thermoresponsive polymer poly(N-vinylisobutyramide) (PNVIBA), Macromolecules 30 (1997) 4499-4501.

[17] K. Heremans, P.T.T. Wong, Pressure effect on the Raman spectrum of proteins: Pressure induced changes in the conformation of lysozyme in aqueous solutions, Chem. Phys. Lett. 118 (1985) 101-104.

[18] K. Heremans, L. Smeller, Protein structure and dynamics at high pressure, Biochim. Biophys. Acta 1368 (1998) 353-370.

[19] Raman C V and Krishnan K S 1928 Nature 121**,** 501.

[20] A. Schulte and Y. Guo, Applications of laser Raman spectroscopy, Handbook of Solid State Spectroscopy, p. 661- 688, Ed. D. R. Vij, Springer (2006)

[21] Chase B 1994 Appl. Spectrosc. 48 14A

[22] McCreery R L 2000 Raman Specctroscopy for Chemical Analysis (New York: Wiley)

[23] Pelletier M 1999 Analytical applications of Raman spectroscopy (Blackwell Science)

[24] Colomban Ph and Corset J.(Eds.) 1999 J. Raman Spectrosc. 30, Special Issue: Raman (Micro) Spectrometry and Materials Science.

[25] Weber W H and Merlin R (Eds.) 2000, Raman Scattering in Materials Science (New York: Springer)

[26] Lord RC and Yu NT, J. Mol. Biol. 50, 509 (1970)